Dear Editor and Reviewers,

We sincerely thank you for the comprehensive and insightful comments on our manuscript. These suggestions are very valuable and significantly improve the quality and clarity of our work. We have carefully addressed all comments raised by the reviewers in a point-by-point manner during the revision. Reviewer comments are shown in *black italics*, our responses are provided in blue, and revised texts in the manuscript are highlighted.

Manuscript title: Classification and quantification of low-visibility events using deep learning over eastern China

MS No.: egusphere-2026-2617

Response to Referee #2 (RC1): General comments:

This study proposes a unified convolutional neural network (CNN) framework that integrates geostationary meteorological satellite observations, meteorological reanalysis data, and $PM_{2.5}$ observations to identify all types of low-visibility events. The framework shows good potential for quantifying the intensity and spatial extent of low-visibility events. In addition, this quantitative framework reveals the nonlinear responses of fog-haze events and population exposure to $PM_{2.5}$ reduction, providing a useful reference for visibility improvement and air quality management. Overall, this study provides a valuable methodological contribution to the monitoring and assessment of low-visibility events. I suggest that the manuscript be accepted after the authors adequately address the specific comments below.

We thank the reviewer for the positive and constructive assessment of our manuscript. In response to the specific comments, we clarified the rationale for the multi-source framework, added input and architecture ablation experiments, expanded the station-to-grid uncertainty analysis, and strengthened station-level validation. We also expanded the analysis of the cold- and warm-season contrasts, quantified the response of fog-haze area and population-weighted exposure to prescribed $PM_{2.5}$ changes, added a separate Discussion section, and rewrote the Conclusion to focus on the main findings.

Specific comments:

1. The discussion in the second paragraph of the Introduction on the development of fog identification methods needs to be further clarified, especially regarding the advantages of machine learning methods in nonlinear feature extraction and multi-source data fusion. In addition, I suggest further focusing on the necessity of integrating satellite spectral data, meteorological reanalysis data, and ground-based $PM_{2.5}$ observations.

We thank the reviewer for this helpful suggestion. We revised the second paragraph of the Introduction to explain how machine-learning methods capture nonlinear interactions among satellite, meteorological and aerosol variables and why these data sources are integrated. Satellite observations provide spatial optical information, meteorological reanalysis constrains conditions associated with low visibility, and ground-based $PM_{2.5}$ observations help distinguish clean fog from polluted fog-haze. The input-ablation results support this strategy. Sat-PM achieved the highest low-visibility F1 score of 0.78, compared with 0.71 for Sat, 0.67 for meteorology-only, 0.53 without meteorology and 0.30 for satellite-only inputs (Table S3).

Lines 65-72:

"By contrast, machine-learning and deep-learning methods can learn nonlinear relationships among multiple variables and may improve detection performance compared with fixed-threshold methods (Shin and Kim, 2018; Jeon et al., 2020; Huang et al., 2022). Model generalization can also benefit from the integration of large-scale multi-source data (Xu et al., 2025). Satellite spectral data capture cloud and aerosol signatures, meteorological reanalysis describes fog-favorable conditions, and ground-based $PM_{2.5}$ indicates aerosol loading. Together, these inputs help distinguish clean fog from polluted fog-haze, which can resemble cloud in satellite imagery (Hutchison et al., 2008)."

Table S3 Performance comparison of input combinations. Accuracy, precision, recall, F1 score, macro F1, and weighted F1 are reported for models using different combinations of satellite, meteorological, and $PM_{2.5}$ inputs.

Model	Accuracy	Clear precision	Clear recall	Clear F1	Low-vis precision	Low-vis recall	Low-vis F1	Macro F1	Weighted F1
Sat-PM	0.93	0.96	0.95	0.96	0.75	0.81	0.78	0.87	0.95
Sat	0.91	0.95	0.94	0.95	0.73	0.69	0.71	0.83	0.94
Satellite only	0.78	0.98	0.78	0.87	0.19	0.77	0.30	0.58	0.83
No meteorology	0.92	0.98	0.93	0.96	0.41	0.74	0.53	0.74	0.93
Meteorology only	0.95	0.99	0.96	0.97	0.56	0.82	0.67	0.82	0.95

2. In Sect. 2.4, the authors are suggested to explain how $PM_{2.5}$ and visibility station data were interpolated or mapped onto the FY-4A grid, how missing values were handled, and whether the use of nearest-neighbor interpolation may introduce spatial uncertainty in regions with sparse monitoring stations.

We thank the reviewer for this helpful suggestion. We revised Sect. 2.4 and Supplementary Text S1 to clarify the station-to-grid mapping and missing-value treatment. At each hour, $PM_{2.5}$ observations and visibility labels were mapped to the 4 km FY-4A grid using the nearest valid station within 150 km. Missing station-derived values were filled only when a valid station was available within this distance, and grid cells farther than 150 km were excluded. We also added Fig. S2 to quantify the resulting spatial uncertainty using station-distance statistics and leave-one-out cross-validation. Valid $PM_{2.5}$ and visibility stations were available within 150 km for 89.4% and 94.0% of the candidate grid cells, respectively. For $PM_{2.5}$, nearest-neighbor interpolation produced an MAE of 10.91 $\mu g\ m^{-3}$, an RMSE of 19.47 $\mu g\ m^{-3}$ and an r of 0.93, compared with 15.78 $\mu g\ m^{-3}$, 29.98 $\mu g\ m^{-3}$ and 0.85 for inverse-distance weighting. The agreement for visibility labels was 0.902 for nearest-neighbor interpolation and 0.913 for inverse-distance weighting. These results quantify the uncertainty associated with sparse station coverage and support the use of nearest-neighbor mapping for the regional analysis.

Line 136-141:

"Because the datasets differ in spatial resolution, sampling frequency, and measurement height, this collocation may introduce representativeness uncertainty. We therefore quantified the station-to-grid uncertainty using nearest-station distance statistics and leave-one-out cross-validation for $PM_{2.5}$ and visibility labels (Fig. S2). Further details of data preprocessing, standardization, and uncertainty evaluation are provided in Text S1."

Text S1 Line 110-120:

"To quantify the uncertainty introduced by station-to-grid collocation, we examined the distance from each grid cell to the nearest valid $PM_{2.5}$ and visibility station and performed leave-one-out cross-validation (LOOCV) for the station-based $PM_{2.5}$ and visibility labels (Fig. S2). For $PM_{2.5}$, 89.4% of grid cells were within 150 km of the nearest valid station, with a 95th-percentile distance of 117.3 km. For visibility stations, 94.0% of grid cells were within 150 km, with a 95th-percentile distance of 94.1 km. In the $PM_{2.5}$ LOOCV, nearest-neighbor interpolation yielded MAE = 10.91 μg m^{-3}, RMSE = 19.47 μg m^{-3}, and r = 0.93, while inverse-distance weighting (IDW) yielded MAE = 15.78 μg m^{-3}, RMSE = 29.98 μg m^{-3}, and r = 0.85. For visibility-label LOOCV, the agreement was 0.902 for nearest-neighbor interpolation and 0.913 for IDW. These results indicate that some uncertainty remains in station-to-grid collocation, but it has limited impact on the main regional-scale LVE classification."

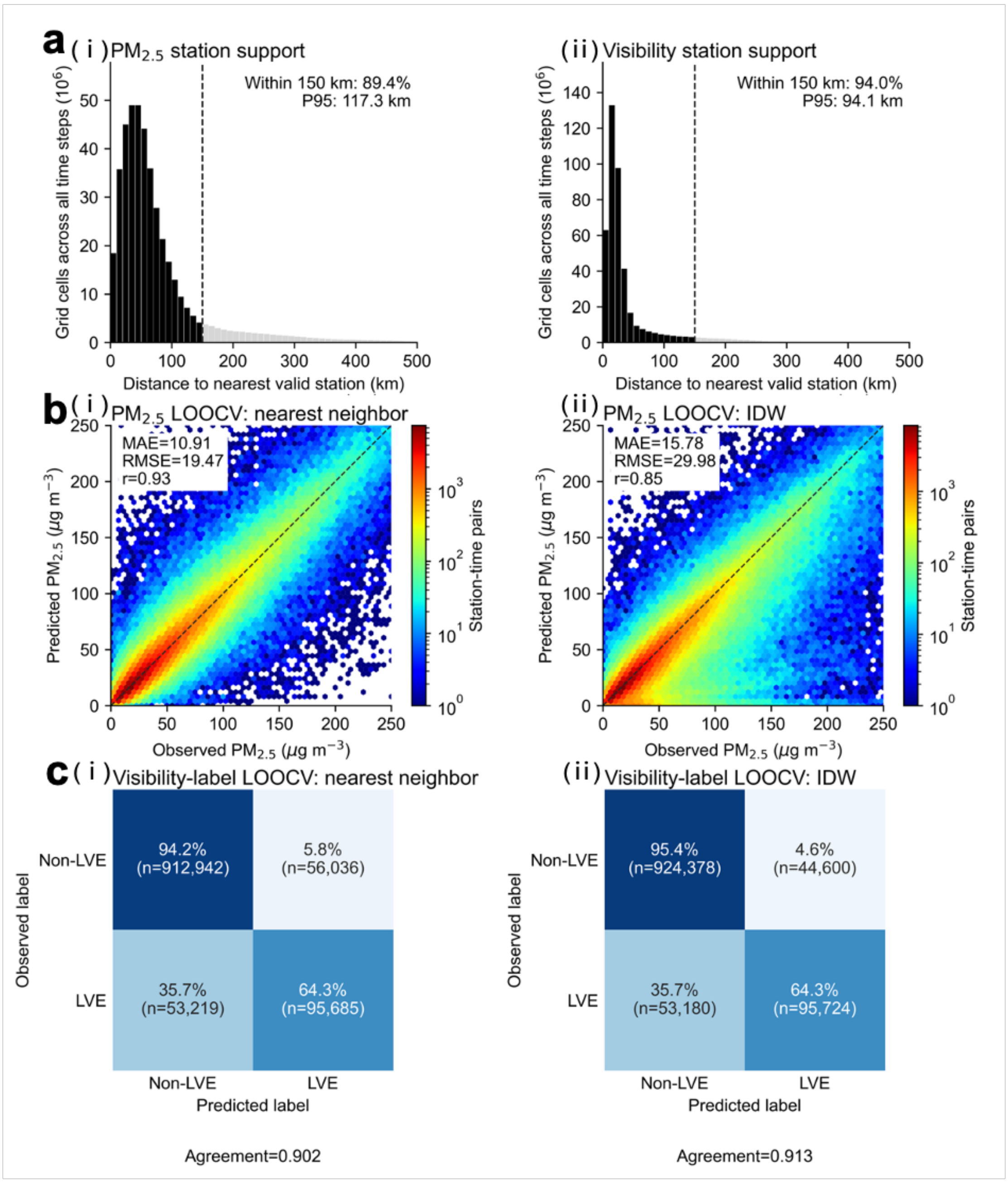

Figure S2 Distance between valid stations and grid cells, and leave-one-out cross-validation (LOOCV) performance for $PM_{2.5}$ and visibility labels. (a) Histograms of the distance from each grid cell to the nearest valid $PM_{2.5}$ station and visibility station. (b) LOOCV for $PM_{2.5}$ using nearest-neighbor and inverse-distance weighting (IDW) interpolation. (c) LOOCV confusion matrices for visibility labels using nearest-neighbor and IDW.

3. In Sect. 4.1, I suggest that the authors supplement the model performance for the classification of different types of low-visibility events.

We thank the reviewer for this helpful suggestion. We clarified that the CNN detects low-visibility versus clear conditions, while individual LVE types are assigned through a subsequent physical attribution step. On independent test data, the terrestrial model achieved an accuracy of 0.93 and a low-visibility F1 score of 0.78, while the maritime model achieved an accuracy of 0.91 and a fog-specific F1 score of 0.71. Separate multiclass scores were not calculated because the station visibility data do not provide independent labels for clean fog, fog-haze and dry haze. This distinction is now clarified in Sects. 3.1 and 4.1.

Lines 147-150:

"The CNN first identifies low-visibility pixels through binary classification against clear conditions. These pixels are then assigned to individual LVE types using physically interpretable environmental criteria."

Lines 245-246:

"Individual LVE types are assigned through the physical attribution described in Sect. 3.1 rather than directly classified by the CNN."

4. In the Results and Discussions section, several typical cases are selected for analysis. I suggest that the authors provide the basis for case selection and explain whether these cases are representative. In addition, if annual results are available, more complete seasonal statistics should be supplemented to enhance the robustness of the conclusions.

We thank the reviewer for this suggestion. We now specify the selection criteria for each case. The 5–6 February 2019 case was selected to capture the complete evolution of co-occurring terrestrial and marine LVEs, from coastal formation to inland and marine expansion and subsequent dissipation (Figs. 2 and 3). The 15 February 2020 case was selected because continuous observations were available at both coastal and inland stations for intensity validation (Fig. 4). The 9 February 2020 case was selected because it contained a widespread winter fog-haze event that clearly revealed the response to prescribed $PM_{2.5}$ reductions (Fig. 6a). These cases illustrate distinct processes and are not used to infer climatological frequencies.

The broader conclusions are supported by independent test events, station-level validation across 821 stations and complete hourly model outputs for the analyzed periods. Among the 821 stations, 62% showed correlations above 0.6 between modelled LVE intensity and observed visibility reduction, while the six scatter plots from different provinces provide representative examples of this spatial evaluation (Figs. S6 and S7). The $PM_{2.5}$ sensitivity analysis uses the complete February hourly series rather than a single event (Fig. 6c–e). The seasonal comparison likewise uses all hourly results for February and July (Fig. 5), which represent contrasting cold- and warm-season regimes. These analyses support the robustness of the conclusions within the study domain and the examined periods. Because a continuous annual climatology was not derived, the revised manuscript does not extend these seasonal conclusions to the full year.

Lines 270-271:

"Figure 3 illustrates the spatiotemporal evolution of the LVE from 15:00 on 5 February to 15:00 on 6 February 2019. This case was selected because it captures co-occurring terrestrial and marine LVEs."

Lines 281-282:

"The 15 February 2020 case was selected because continuous observations were available at both coastal and inland stations."

Lines 304-306:

"All hourly results for February and July 2020 were selected to represent the cold and warm seasons, respectively."

Lines 359-361:

"The fog-haze area change corresponding to the $PM_{2.5}$ change for the whole month is shown in Fig. 6c. The quantitative sensitivity analysis uses all hourly results for February."

5. In Fig. 4b, the authors compare the sea fog intensity simulated by the Sat model with the visibility reduction observed at Dinghai, Putuo, and Shengsi stations. However, the Sat model result in the figure seems to be shown as only one unified simulated value. Since the three stations are located at different spatial positions and the model output is gridded sea fog intensity, the simulated intensity should theoretically be extracted separately from the corresponding or nearest grid cells of each station for comparison.

We thank the reviewer for pointing this out. We agree that the three stations should be compared with model outputs extracted from their respective FY-4A grid cells. We therefore extracted the Sat model intensity from the nearest grid cell for Dinghai, Putuo and Shengsi and added separate station comparisons in the Supplementary Information (Fig. S8). The three comparisons capture the main observed sea fog episodes and show broadly consistent temporal variations, while also revealing local differences among the stations.

The model curve in Fig. 4b(i) is retained to summarize the regional evolution of the sea fog event, rather than to represent any individual station. It is calculated as the arithmetic mean of the three grid cell intensities matched to the stations and is labelled accordingly in the revised manuscript. This regional average evaluates the common temporal signal across the Zhoushan station network while reducing the influence of local fluctuations and differences between station observations and grid cell values. The station comparisons in Fig. S8 provide the corresponding spatially resolved validation and clarify the relationship between the regional average shown in Fig. 4b(i) and the three individual stations. The corresponding station comparisons for land fog in Fig. 4b(ii) are provided in Fig. S9.

Lines 288-290:

"The model curves in Fig. 4b(i) and (ii) are the arithmetic means of the model intensities extracted from the FY-4A grid cells nearest to the corresponding three sea fog and land fog stations, respectively. They provide regional summaries rather than intensities for individual stations. Separate station comparisons are provided in Figs. S8 and S9, respectively."

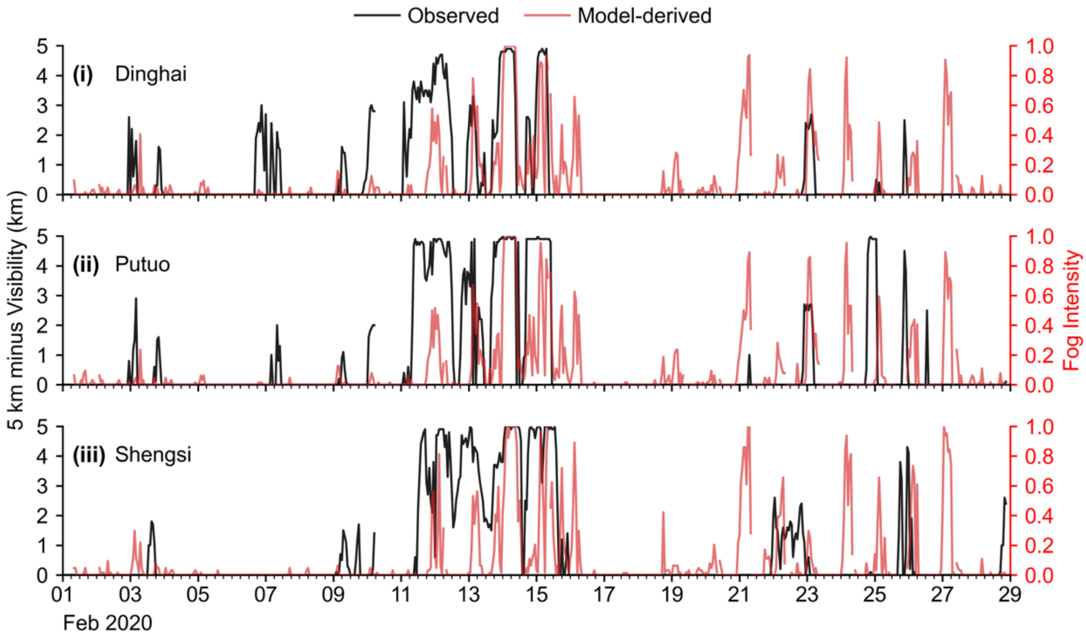

Figure S8 Station-specific comparison of observed visibility reduction and model-derived sea fog intensity at Dinghai (i), Putuo (ii) and Shengsi (iii) during February 2020. Black curves show the observed visibility reduction, calculated as 5 km minus the observed visibility, and red curves show the model derived fog intensity extracted from the nearest FY-4A grid cell for each station.

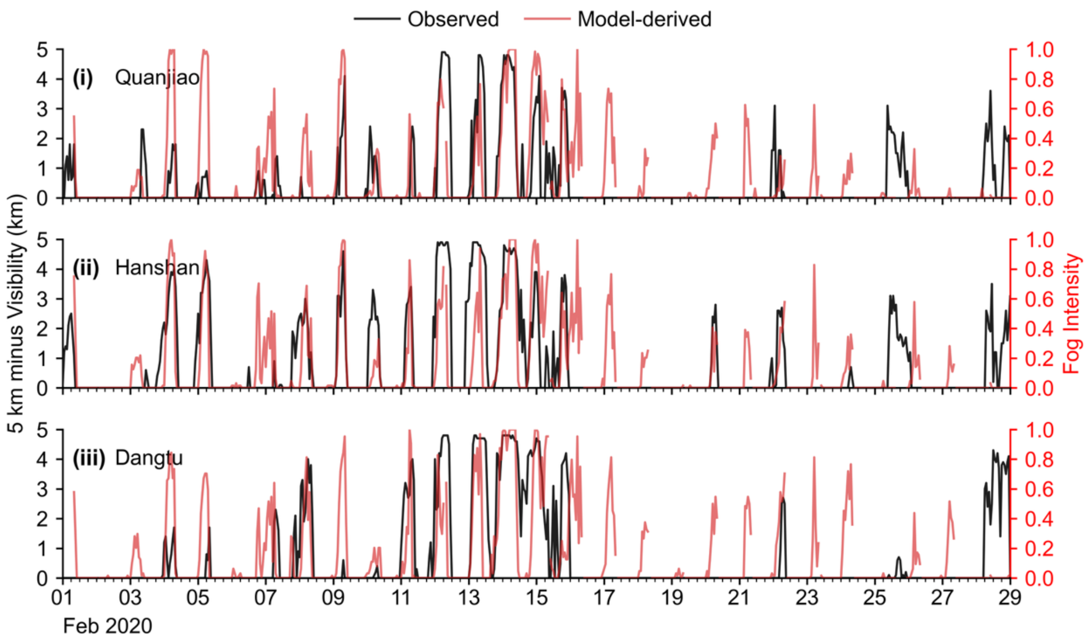

Figure S9 Same as Fig. S8, but for land fog at Quanjiao (i), Hanshan (ii) and Dangtu (iii).

6. I suggest that the authors further discuss the reasons for the seasonal differences in the area of low-visibility events.

We thank the reviewer for this suggestion. We have added the reasons for the seasonal differences in LVE area to the Discussion.

Lines 412-430:

"Seasonal controls differed among LVE types. Winter land fog reached a larger maximum area than summer land fog. Stronger radiative cooling in winter promoted near-surface saturation and favored extensive fog formation (Roach et al., 1976; Mason, 1982). However, cumulative land-fog coverage was similar in the two seasons. More frequent fog formation under moist summer coastal conditions compensated for the smaller event size. Thus, season affected the maximum extent of land fog more strongly than its cumulative coverage. Land fog-haze and dry haze showed stronger winter enhancement. Weak boundary-layer ventilation favours aerosol accumulation during winter. The larger winter fog-haze coverage therefore reflects both favourable saturation conditions and higher aerosol loading. Winter haze was largest at night and in the early morning. Boundary-layer growth after sunrise promoted vertical mixing and pollutant dilution. Unlike winter haze, summer haze increased after sunrise and peaked from late morning to midday. This daytime maximum is consistent with enhanced photochemical production under stronger solar radiation (Sun et al., 2016; Wu et al., 2024). Sea fog persisted longer in summer than in winter. Winter sea fog mainly dissipated after sunrise, whereas summer sea fog often continued into midday. The slower summer dissipation is consistent with the weak diurnal variation of the sea surface and the stability of the marine boundary layer, which reduces the immediate effect of daytime solar heating (Ma et al., 2014; Wagh et al., 2021). These results show that land fog, land fog-haze, dry haze and sea fog should not be treated as a single low-visibility phenomenon."

7. In Lines 346-357, I suggest that the authors supplement quantitative results on the response of fog-haze area to $PM_{2.5}$ reduction.

We thank the reviewer for this helpful suggestion. We added quantitative results in Sect. 4.4 showing that reducing $PM_{2.5}$ to 80%, 60% and 40% of its original level decreased the mean February fog haze area by approximately 43%, 75% and 95%, respectively (Fig. 6e).

Lines 362-366:

"Relative to the baseline, reducing $PM_{2.5}$ to 80%, 60% and 40% of its original level decreased the mean February fog-haze area by approximately 43%, 75% and 95%, respectively (Fig. 6e). The reduction to 80% consistently lowered the event peaks, whereas the reduction to 60% suppressed most large scale fog-haze events."

8. In Lines 371-378, the authors show that reducing winter $PM_{2.5}$ concentrations to 40% leads to simulated fog-haze areas that are highly consistent with the summer results. I suggest that the authors further clarify whether this sensitivity experiment controlled for or considered seasonal differences in meteorological conditions.

We thank the reviewer for this suggestion. We clarified in Sect. 4.4 that only the winter $PM_{2.5}$ input was scaled, while all satellite and meteorological inputs remained unchanged. The experiment therefore evaluates the $PM_{2.5}$ response under fixed winter meteorological conditions. The agreement with the observed summer distribution indicates the contribution of aerosol loading to the seasonal contrast in fog haze area, rather than reproducing the full summer conditions.

Lines 386-390:

“Only the winter $PM_{2.5}$ input was scaled, while all satellite and meteorological inputs remained unchanged. The experiment therefore evaluates the $PM_{2.5}$ response under fixed winter meteorological conditions. The agreement with the observed summer distribution indicates the contribution of aerosol loading to the seasonal contrast in fog haze area, rather than reproducing full summer conditions.”

9. In Line 404, the main text states that the “mean fog-haze area declined by 42%”, whereas the value labeled in Fig. 6e seems to be 43%. I suggest that the authors check the consistency between the value in the main text and that in the figure.

We thank the reviewer for noting this inconsistency. We corrected the main text to **43%** to match Fig. 6e.

Lines 24-27:

“Based on the model, we are able to investigate the environmental policy to reduce fog-haze and the corresponding population exposure. Over eastern China, a 20% reduction of overall $PM_{2.5}$ can reduce the fog-haze area by 43% in winter.”

Lines 397-398:

“Reducing $PM_{2.5}$ from 100% to 80% of its original level decreased the mean fog-haze area by 43%, but reduced population exposure by only 15%.”

Technical corrections:

1. Line 38: There is a formatting error with double parentheses in “transportation safety ((Ord Us Epa...”.

We thank the reviewer for noting this error. The obsolete citation and double parentheses have been removed from the revised manuscript.

2. The capitalization style of words in the section headings should be made consistent throughout the manuscript.

We thank the reviewer for noting this issue. We have standardized the capitalization of all section headings throughout the manuscript.

Line 84:

“2 Data and observations”

Line 85:

“2.1 Study region”

Line 91:

“2.2 Multi-source observational datasets”

Line 115:

“2.3 Visibility definition and LVE labelling”

Line 204:

“3.3 Model training and validation”

Line 240:

"**4.1 Overall performance of models**"

Reference:

Huang, Y., Wu, M., Guo, J., Zhang, C., and Xu, M.: A Correlation Context-Driven Method for Sea Fog Detection in Meteorological Satellite Imagery, IEEE Geoscience and Remote Sensing Letters, 19, 1–5, https://doi.org/10.1109/LGRS.2021.3095731, 2022.

Hutchison, K. D., Iisager, B. D., Kopp, T. J., and Jackson, J. M.: Distinguishing aerosols from clouds in global, multispectral satellite data with automated cloud classification algorithms, J. Atmos. Oceanic Technol., 25, 501–518, https://doi.org/10.1175/2007JTECHA1004.1, 2008.

Jeon, H.-K., Kim, S., Edwin, J., and Yang, C.-S.: Sea Fog Identification from GOCI Images Using CNN Transfer Learning Models, Electronics, 9, 311, https://doi.org/10.3390/electronics9020311, 2020.

Ma, N., Zhao, C., Chen, J., Xu, W., Yan, P., and Zhou, X.: A novel method for distinguishing fog and haze based on PM2.5, visibility, and relative humidity, Sci. China Earth Sci., 57, 2156–2164, https://doi.org/10.1007/s11430-014-4885-5, 2014.

Mason, J.: The Physics of Radiation Fog, Journal of the Meteorological Society of Japan. Ser. II, 60, 486–499, https://doi.org/10.2151/jmsj1965.60.1_486, 1982.

Roach, W. T., Brown, R., Caughey, S. J., Garland, J. A., and Readings, C. J.: The physics of radiation fog: I – a field study, Quarterly Journal of the Royal Meteorological Society, 102, 313–333, https://doi.org/10.1002/qj.49710243204, 1976.

Shin, D. and Kim, J.-H.: A New Application of Unsupervised Learning to Nighttime Sea Fog Detection, Asia-Pacific J Atmos Sci, 54, 527–544, https://doi.org/10.1007/s13143-018-0050-y, 2018.

Sun, Y., Jiang, Q., Xu, Y., Ma, Y., Zhang, Y., Liu, X., Li, W., Wang, F., Li, J., Wang, P., and Li, Z.: Aerosol characterization over the North China Plain: Haze life cycle and biomass burning impacts in summer, Journal of Geophysical Research: Atmospheres, 121, 2508–2521, https://doi.org/10.1002/2015JD024261, 2016.

Wagh, S., Krishnamurthy, R., Wainwright, C., Wang, S., Dorman, C. E., Fernando, H. J. S., and Gultepe, I.: Study of Stratus-Lowering Marine-Fog Events Observed During C-FOG, Boundary-Layer Meteorol, 181, 317–344, https://doi.org/10.1007/s10546-021-00670-w, 2021.

Wu, Y., Liu, Q., Liu, D., Tian, P., Xu, W., Wang, J., Hu, K., Li, S., Jiang, X., Wang, F., Huang, M., Ding, D., Yu, C., and Hu, D.: Enhanced formation of nitrogenous organic aerosols and brown carbon after aging in the planetary boundary layer, npj Clim Atmos Sci, 7, 179, https://doi.org/10.1038/s41612-024-00726-x, 2024.

Xu, M., Chen, K., Guo, H., Huang, Y., Wu, M., Shi, Z., Zhang, C., and Guo, J.: MFogHub: bridging multi-regional and multi-satellite data for global marine fog detection and forecasting, 2025.

Response to Referee #1 (RC2):

This study introduces a unified convolutional neural network (CNN) framework that integrates the geostationary satellite, meteorology, and fine particulate matter ($PM_{2.5}$) observation data to identify all types of LVEs. The classified and quantified LVEs, along with the established relationship with pollution, explicitly guide the air-quality policy for the co-benefits of improving air visibility and human health.

Overall, observations are not presented properly, fog definition is missing, Vis is not only due to fog but many others hydrometeors (see Gultepe et al 2019 PAAG, Nature). Conclusions are not clear to me, see comments below. You need a discussion section also, presently missing.

We thank the reviewer for the constructive assessment. In response, we revised the manuscript to clarify the LVE definition and to better acknowledge the possible contribution of non-fog hydrometeors. We added station-level validation and uncertainty analyses, and expanded the Discussion where the seasonal variability and $PM_{2.5}$ sensitivity are interpreted. We also rewrote the Conclusions so that they follow the main findings more closely, and updated the figures and Supplementary material accordingly. These changes strengthen the clarity and evidential support of the manuscript.

Deep learning ML application needs to be clarified, why you selected the one you used? What is the uncertainty of its usage? What are the issues related to various fog types and training analysis? How good it is and how can input can affect the outcome, uncertainties? You need more focused on the conclusions.

We thank the reviewer for this important comment. We added ablation experiments to clarify both the input choice and model selection (Tables S3 and S4). The Sat-PM model achieved the best low-vis F1 score (0.78), outperforming Sat (0.71), meteorology-only (0.67), no-meteorology (0.53), and satellite-only (0.30), showing that multi-source fusion, especially $PM_{2.5}$, improves low-visibility detection (Table S3). The architecture comparison also supports the selected Sat model, which achieved the highest accuracy (90.95%) and a balanced low-visibility and clear-class performance among the tested models (Table S4).

Table S3 Performance comparison of input combinations. Accuracy, precision, recall, F1 score, macro F1, and weighted F1 are reported for models using different combinations of satellite, meteorological, and $PM_{2.5}$ inputs.

Model	Accuracy	Clear precision	Clear recall	Clear F1	Low-vis precision	Low-vis recall	Low-vis F1	Macro F1	Weighted F1
Sat-PM	0.93	0.96	0.95	0.96	0.75	0.81	0.78	0.87	0.95
Sat	0.91	0.95	0.94	0.95	0.73	0.69	0.71	0.83	0.94
Satellite only	0.78	0.98	0.78	0.87	0.19	0.77	0.30	0.58	0.83
No meteorology	0.92	0.98	0.93	0.96	0.41	0.74	0.53	0.74	0.93
Meteorology only	0.95	0.99	0.96	0.97	0.56	0.82	0.67	0.82	0.95

Table S4 Performance comparison of the Sat model with baseline configurations. The table lists key performance metrics (Accuracy, Recall, and Precision) for the proposed Sat model against three ablation study baselines: a standard CNN (no attention), a CNN with only channel attention, and a CNN with only spatial attention. Metrics are provided for both 'low-visibility' and 'clear' classes.

Model	Accuracy	low-visibility Recall	low-visibility Precision	clear Recall	clear Precision
Sat (Ours)	90.95%	69%	73%	94%	95%
CNN (no attention)	89.71%	71%	67%	93%	94%
CNN (channel attention)	89.87%	70%	68%	94%	94%
CNN (spatial attention)	89.25%	67%	67%	94%	94%

Major/minor issues:

1. Line 37/38: See Gultepe studies for low-visibility conditions and cold fog/ice fog; you are only using a simple definition of low-visibility conditions. This can include drizzle, rain, snow, ice fog, etc.

We thank the reviewer for this helpful comment. We revised the definition at Lines 37-38 to clarify that LVEs are operationally defined by reduced near-surface visibility and may include fog, haze, fog-haze mixtures, drizzle, rain, snow, ice fog, and other mixed hydrometeor conditions, following the recommendation by Gultepe studies. In the revision, we further examined the weather records in our samples. The results show that fog is the dominant category for near-surface visibility <= 2 km, accounting for 59% of the coastal and 73% of the inland records for 2412 stations (Fig. S6a). Rain contributed to the second important fraction, which contained fogs with some precipitations (Wang et al., 2021), which is 18% and 17% for inland and coastal sites, respectively. The other weather types contributed to <5% of the weather events. We acknowledge that the classified fog has contained some precipitations, and added related discussions in the revision. Considering the aim of our study is to identify the low-visibility events but not the detailed weather types, the precipitating fogs have not been separately trained for the model.

Lines 37-44:

"Low-visibility events (LVEs) occur across both terrestrial and marine environments. LVEs are defined by reduced near-surface visibility and can be associated with fog, haze, fog-haze mixtures, drizzle, rain, snow, ice fog, and other mixed hydrometeor conditions (Gultepe et al., 2007b, 2015, 2019). The weather records are analyzed from 2412 stations in February (Fig. S6a), showing fog contributed to 73% and 59% of weather types for inland and coastal sites, respectively. Rain contributed to the second important weather types, with 18% and 17% for inland and coastal sites, while the others are <5%. The classified fog in this study therefore may contain some precipitation, but has not been further separated."

Lines 118-119:

"Fig. S6a shows the near-surface low visibility is governed primarily by fog droplets, aerosol particles, and other hydrometeors."

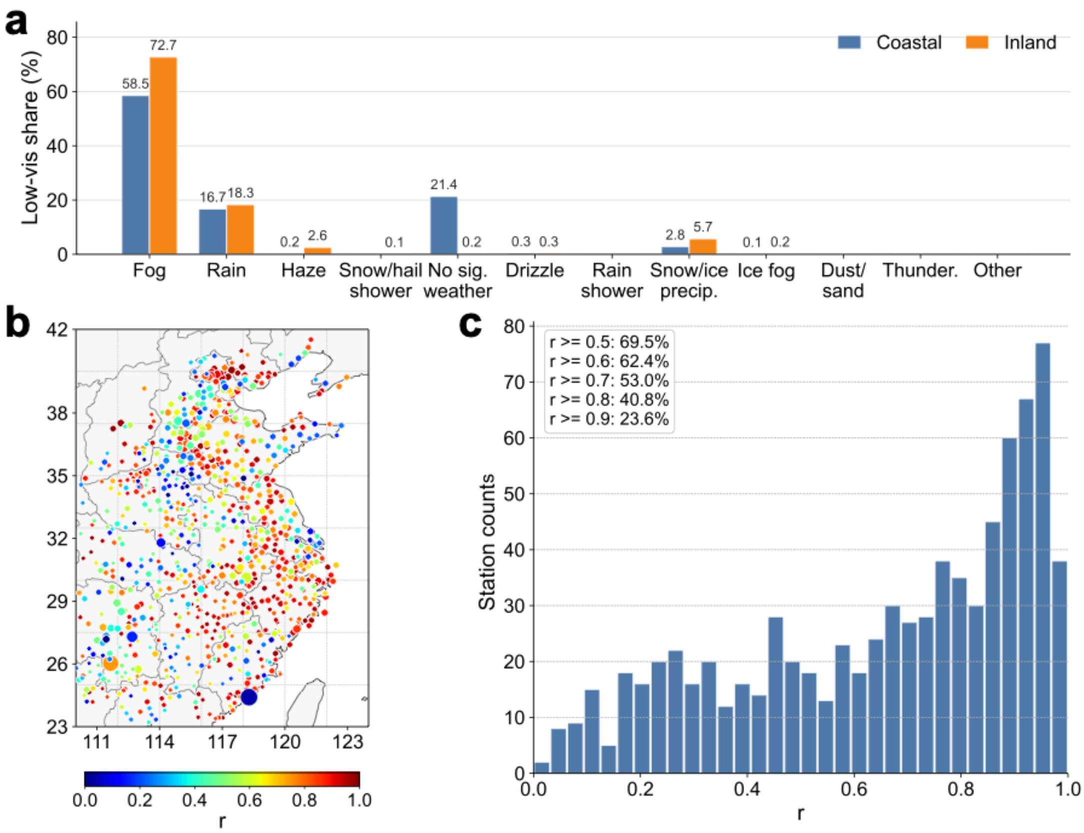

Figure S6 Low-visibility weather composition and station-level validation in February 2020. (a) Present-weather category shares during low-visibility records in coastal and inland stations. (b) Spatial distribution of station-level correlation between model-derived fog intensity and observed visibility reduction. (c) Histogram of station-level correlation coefficients for 821 validation stations.

Lines 162-165:

"Consistent with the operational definition in Sect. 2.3, we did not further subdivide LVEs by precipitation occurrence, because drizzle, weak precipitation, and fog often co-occur and rain-only cases generally do not represent the LVEs targeted here (Wang et al., 2021)."

2. Line 48: See Gultepe et al. for satellite use for fog (JAM).

We revised the Introduction to cite Gultepe et al. (2007) more explicitly and to clarify that satellite-based fog detection is limited by night-time conditions, high-level clouds, and the need for auxiliary screen-temperature information.

Lines 54-58:

"The use of satellite observations for fog detection is often limited by the absence of visible channels at night and by contamination from mid- and high-level clouds. Traditional fog identification relies on fixed thresholds applied to one or more parameters, which can be difficult to generalize across changing surface and cloud conditions (Ellrod, 1995; Eyre et al., 1984; Gultepe et al., 2007a)."

3. Line 67: see Gultepe et al 2018 Atmos Res. paper for fog types and low vis conditions.

This paper is now discussed and cited in the revised manuscript. We have added the recommended *Atmos Res.* citation (Gultepe et al., 2015) and revised the sentence to better reflect the broader range of low-visibility conditions and fog types.
Lines 75-78:

"Given these detection challenges, only a limited number of studies have addressed the broader range of LVE types, including land and sea fog, unpolluted and polluted fog, and other mixed hydrometeor conditions, thereby examining their interactions and transitions (Gultepe et al., 2007b, 2015, 2019)."

4. Section 2.2: Integration of $PM_{2.5}$, ERA5, and satellite data can have various issues. What is the uncertainty in this process?

We thank the reviewer for pointing this out. We have now revised Sect. 2.4 and Text S1 to describe the temporal matching, spatial collocation, missing-value treatment, and nearest-neighbor mapping more clearly. We also added Fig. S2 to quantify the uncertainty introduced by station-to-grid collocation using nearest-station distance statistics and leave-one-out cross-validation (LOOCV) for $PM_{2.5}$ and visibility labels.

Lines 112-114:

"The temporal matching, spatial collocation, and uncertainty evaluation of these multi-source datasets are described in Sect. 2.4 and Supplementary Text S1."

Line 136-141:

"Because the datasets differ in spatial resolution, sampling frequency, and measurement height, this collocation may introduce representativeness uncertainty. We therefore quantified the station-to-grid uncertainty using nearest-station distance statistics and leave-one-out cross-validation for $PM_{2.5}$ and visibility labels (Fig. S2). Further details of data preprocessing, standardization, and uncertainty evaluation are provided in Text S1."

Text S1 Line 110-120:

"To quantify the uncertainty introduced by station-to-grid collocation, we examined the distance from each grid cell to the nearest valid $PM_{2.5}$ and visibility station and performed leave-one-out cross-validation (LOOCV) for the station-based $PM_{2.5}$ and visibility labels (Fig. S2). For $PM_{2.5}$, 89.4% of grid cells were within 150 km of the nearest valid station, with a 95th-percentile distance of 117.3 km. For visibility stations, 94.0% of grid cells were within 150 km, with a 95th-percentile distance of 94.1 km. In the $PM_{2.5}$ LOOCV, nearest-neighbor interpolation yielded MAE = 10.91 μg m^{-3}, RMSE = 19.47 μg m^{-3}, and r = 0.93, while inverse-distance weighting (IDW) yielded MAE = 15.78 μg m^{-3}, RMSE = 29.98 μg m^{-3}, and r = 0.85. For visibility-label LOOCV, the agreement was 0.902 for nearest-neighbor interpolation and 0.913 for IDW. These results indicate that some uncertainty remains in station-to-grid collocation, but it has limited impact on the main regional-scale LVE classification."

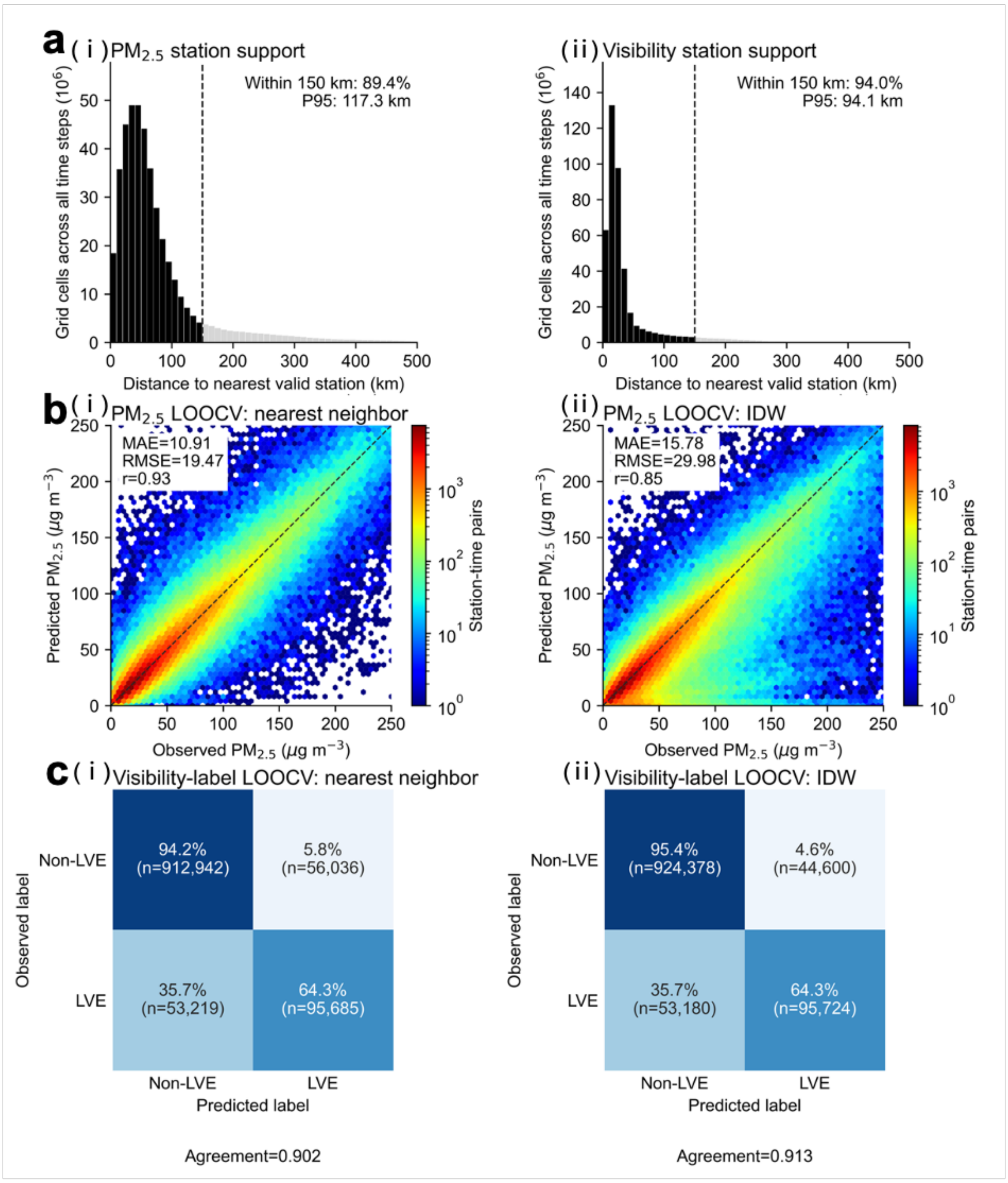

Figure S2 Distance between valid stations and grid cells, and leave-one-out cross-validation (LOOCV) performance for $PM_{2.5}$ and visibility labels. (a) Histograms of the distance from each grid cell to the nearest valid $PM_{2.5}$ station and visibility station. (b) LOOCV for $PM_{2.5}$ using nearest-neighbor and inverse-distance weighting (IDW) interpolation. (c) LOOCV confusion matrices for visibility labels using nearest-neighbor and IDW.

5. Line 135: These definitions may not be correct because fog can occur over large-size aerosols also. Discuss this.

We agree with reviewer that fog can occur over a broader aerosol size spectrum. We revised Sect. 3.1 to clarify that $PM_{2.5}$ is used to identify the polluted fogs, rather than being an illustration for fog formation. The fog-haze represents the polluted fog containing more aerosols.

Lines 155-158:

"This $PM_{2.5}$-based separation is to identify polluted fogs, rather than a microphysical definition of fog formation. In particular, the fog-haze category represents water-saturated, fog-favorable conditions under higher aerosol loading, to denote the fog occurring under higher aerosol conditions."

6. Section 3.2: Averaging of all data in different areas with various pixel numbers can lead to large uncertainty. Did you look at the errors among them? Provide this.

We thank reviewer for this comment. We now clarified that the model input is the full 64 × 64 spatial matrices for each variable, rather than an averaged value over a region. The averaging in Sect. 3.2 refers only to pooling within the attention module, used to derive attention weights inside each tensor, and does not replace the spatial input or average across regions with different pixel numbers.

Lines 134-136:

"The collocated variables were retained as fixed-size 64 × 64 tensors on the FY-4A grid, rather than being averaged across regions with different pixel numbers."

Lines 190-195:

"The spatial attention module uses average pooling together with max pooling within each 64 × 64 input tensor, followed by a 7 × 7 convolution kernel to focus on informative regions, effectively distinguishing fog boundaries from complex underlying surfaces (Woo et al., 2018). In both branches, pooling is used only inside the attention module to derive attention weights and does not replace the spatial input or average across different regions."

7. Verification; Needs scatter plots of various parameters from each platform; this can show the bias in the estimations.

We have now added Fig. S6b, c to provide station-level validation of model-derived fog intensity against observed visibility reduction (5 km - Vis) across 821 stations, as reply to comment 1. These diagnostics show the spatial distribution and overall spread of the correlations.

Lines 292-294:

"The correlations between model-derived fog intensity and observed visibility reduction (5 km - Vis) are shown for 821 validation stations in Fig. S6b, c, showing 62% of the stations have $r > 0.6$, validating the model performance to predict LVE intensity."

8. Fig. 4; y axis values as model??? Doesn't clear. (ii) plots show the scatter plots but they don't have good trends. It tells me large diffs between obs and predicted ones. But plots are not clear anyway….

We revised the axis labels and caption of Fig. 4 to clarify that the y-axis shows the model-derived fog intensity, normalized from 0 to 1, rather than a direct visibility prediction. We also added representative station-level scatter plots between model fog intensity and observed visibility reduction, defined as 5000 m − Vis, in Fig. S7. These plots show clear positive relationships across six stations from different provinces, with correlation coefficients of 0.87–

0.94. This supports the model's ability to capture the visibility-reduction signal.

Lines 280-294:

"To further evaluate model performance, we compared the simulated LVE intensity with ground-station visibility observations. The 15 February 2020 case was selected because continuous observations were available at both coastal and inland stations. Fig. 4a shows the spatiotemporal evolution of a representative fog event on 15 February 2020, together with the locations of the validation stations. The model captures the main evolution of the fog, although some local mismatches are expected because of the uncertainty in model spatial resolution. Fig. 4b(i) and (ii) show the temporal evolution at representative sea-fog and land-fog stations, respectively. At both coastal and inland sites, the simulated intensity generally follows the observed visibility reduction. The model curves in Fig. 4b(i) and (ii) are the arithmetic means of the model intensities extracted from the FY-4A grid cells nearest to the corresponding three sea fog and land fog stations, respectively. They provide regional summaries rather than intensities for individual stations. Separate station comparisons are provided in Figs. S8 and S9, respectively. The correlations between model-derived fog intensity and observed visibility reduction (5 km - Vis) are shown for 821 validation stations in Fig. S6b, c, showing 62% of the stations have r > 0.6, validating the model performance to predict LVE intensity."

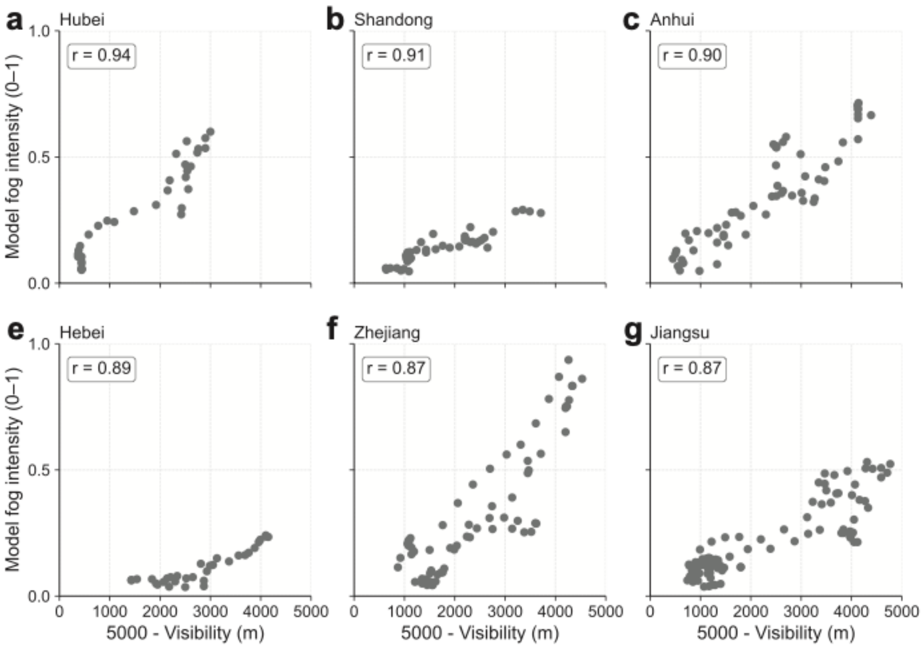

Figure S7 Station-level validation of model fog intensity. Scatter plots of model fog intensity versus observed visibility reduction (5000 m − Vis) for six representative stations from different provinces in February 2020. Correlation coefficients are shown in each panel.

9. Areal coverage comparisons seem acceptable, but the errors in Fig. 4 indicate that there are large uncertainties in the simulations.

The figure has been updated as replied to the above comments.

10. Fig3; shows images but I need to see scatter plots of Vis observed versus others.

We thank the reviewer for this suggestion. Fig. 3 is a qualitative example of the LVE spatial pattern. As described in our responses to Comments 7 and 8, we added quantitative station-level validation in Figs. S6 and S7, where Fig. S6 shows the spatial distribution and histogram of the correlation between model-derived fog intensity and observed visibility reduction (5000 m - Vis) across 821 stations, and Fig. S7 provides scatter plots for six representative stations from different provinces.

11. Conclusions; You said this "Anchored by ground-station visibility data as the target truth, the framework achieved an identification accuracy exceeding 90%. Crucially, by integrating PM2.5 data, the model successfully disentangled the microphysical pathways of different LVEs, solving a persistent challenge in remote sensing over complex terrestrial and coastal environments." But fig4 shows completely different. If correlation 60% how can you get accuracy 90%?

The >90% expresses the accuracy for the detection of low-visibility over clear conditions, but not the correlation between fog intensity and visibility. The intensity–visibility relationship is evaluated separately in Figs. S6 and S7. We have now clarified this in the revised text.

Lines 242-248:

"This accuracy reflects the binary classification of low-visibility versus clear conditions, whereas the correlation between modelled LVE intensity and observed visibility is evaluated in Figs. S6 and S7. Individual LVE types are assigned through the physical attribution described in Sect. 3.1 rather than directly classified by the CNN. In parallel, the maritime Sat model proved robust for sea fog detection, securing an accuracy of 0.91 and a fog-specific F1-score of 0.71. Tables S3 and S4 provide the input-ablation and architecture comparisons, respectively."

12. Itemize your conclusions clearly. What are the findings? To me this section is not written properly based on findings.

We thank the reviewer for this comment. We have rewritten the Conclusion to make the main findings clearer.

Lines 466-485:

"**6 Conclusion**

This study developed and validated a framework that integrates satellite observations, reanalysis meteorological data and ground-based air-quality data to identify and quantify low visibility events over eastern China. By distinguishing clean fog, polluted fog-haze, dry haze and sea fog, the framework resolves the relative roles of near-surface saturation and aerosol loading in regional visibility loss. The prescribed $PM_{2.5}$ experiments show that pollution control can change both the extent and the category of low visibility events. When saturation near the surface persists, polluted fog-haze may shift towards cleaner fog rather than disappear. This response is consistent with aerosol effects on optical extinction and aqueous processing (Zhong et al., 2018; Peng et al., 2021).

A further insight is that regional visibility improvement does not necessarily lead to a comparable reduction in population exposure. Initial reductions in fog-haze coverage can occur mainly in less populated areas, while substantial exposure remains in densely populated emission hotspots. This spatial concentration is relevant to health assessment because humid aerosol processing may increase the soluble fraction and potential biological availability of particulate matter (Pope III and Dockery, 2006; Miller et al., 2017; Wang et al., 2020). Air quality assessments should therefore combine LVE attribution with population weighting instead of using visibility improvement alone as a proxy for reduced exposure or health benefit. Integrating this framework with models that couple atmospheric chemistry and meteorology, together with health data, could extend LVE analysis from retrospective diagnosis to prospective evaluation of clean air policies."

13. Also you need a clear discussion section, presently it is missing.

We have adopted reviewer's suggestion and added a discussion section in the revision.

Lines 403-464:

"5 Discussion

Independent test data and station observations support the application of the multi-source framework to regional LVE classification and intensity mapping. Station-level correlations between modelled LVE intensity and observed visibility reduction further show that the output represents event intensity rather than only binary low-visibility conditions (Figs. S6b, c and S7). The ablation experiments also show that satellite, meteorological and $PM_{2.5}$ data provide complementary information. Removing $PM_{2.5}$ reduced the performance of land low-visibility detection, whereas the attention-based CNN provided the most balanced performance among the tested architectures (Tables S3 and S4).

Seasonal controls differed among LVE types. Winter land fog reached a larger maximum area than summer land fog. Stronger radiative cooling in winter promoted near-surface saturation and favored extensive fog formation (Roach et al., 1976; Mason, 1982). However, cumulative land-fog coverage was similar in the two seasons. More frequent fog formation under moist summer coastal conditions compensated for the smaller event size. Thus, season affected the maximum extent of land fog more strongly than its cumulative coverage. Land fog-haze and dry haze showed stronger winter enhancement. Weak boundary-layer ventilation favours aerosol accumulation during winter. The larger winter fog-haze coverage therefore reflects both favourable saturation conditions and higher aerosol loading. Winter haze was largest at night and in the early morning. Boundary-layer growth after sunrise promoted vertical mixing and pollutant dilution. Unlike winter haze, summer haze increased after sunrise and peaked from late morning to midday. This daytime maximum is consistent with enhanced photochemical production under stronger solar radiation (Sun et al., 2016; Wu et al., 2024). Sea fog persisted longer in summer than in winter. Winter sea fog mainly dissipated after sunrise, whereas summer sea fog often continued into midday. The slower summer dissipation is consistent with the weak diurnal variation of the sea surface and the stability of the marine boundary layer, which reduces the immediate effect of daytime solar heating (Ma et al., 2014; Wagh et al., 2021). These results show that land fog, land fog-haze, dry haze and sea fog should not be treated as a single low-visibility phenomenon.

The $PM_{2.5}$ sensitivity experiments clarify the seasonal contrast in fog-haze. They quantify the response of fog-haze to prescribed changes in aerosol loading. Reducing winter $PM_{2.5}$ to 40%

of its original level shifted the simulated cumulative distribution of fog-haze area towards the observed summer distribution. Increasing summer $PM_{2.5}$ to 250% produced a distribution closer to the observed winter distribution (Fig. 6d). These results suggest that aerosol loading contributes substantially to the larger winter fog-haze coverage. Under comparable saturation and liquid-water conditions, higher aerosol loading can increase CCN abundance and favour the formation of more numerous, smaller droplets. The larger total droplet surface area enhances light extinction (Twomey, 1977; Jia et al., 2026). Humid conditions promote aerosol hygroscopic growth and aqueous-phase processing, which can further increase particle mass and extinction (Peng et al., 2021; Zhong et al., 2018). Under real atmospheric conditions, aerosol–radiation interactions can reduce surface heating and suppress boundary-layer growth. This effect can promote the accumulation of aerosols and moisture near the surface (Wu et al., 2019). The associated meteorological feedback is not represented because the meteorological fields were fixed. Under persistent saturation, lower $PM_{2.5}$ weakens aerosol-related extinction and reduces CCN-rich conditions. Consistent with the increased clean-fog coverage in Fig. S5, the model therefore reclassifies some fog-haze pixels as clean fog rather than clear conditions.

Fog-haze area and population exposure responded differently to $PM_{2.5}$ reduction (Fig. 6e). During the initial reduction stage, fog-haze area declined more rapidly than population exposure. Exposure became more responsive when $PM_{2.5}$ fell to approximately 60% or below its original level. This lag resulted from the population weighting of the exposure metric. Initial reductions mainly removed fog-haze from less populated regions with weaker anthropogenic emissions, while the remaining events persisted in densely populated emission hotspots. After $PM_{2.5}$ had been reduced by more than 40%, an additional 10% reduction produced an 18% decrease in population exposure. The 40% reduction therefore represents an effective range under the tested winter conditions, rather than a universal critical threshold.

The spatial concentration of fog-haze in densely populated emission regions is relevant to potential population exposure. Under humid conditions, aqueous-phase processing promotes the formation of water-soluble secondary aerosols (Wang et al., 2020). These aerosol components may be more bioavailable after inhalation and may contribute to systemic effects (Pope III and Dockery, 2006; Miller et al., 2017). The population-weighted fog-haze intensity should therefore be interpreted as an indicator of potential exposure, not as a direct epidemiological estimate of health risk.”

Reference:

Ellrod, G. P.: Advances in the detection and analysis of fog at night using GOES multispectral infrared imagery, Weather Forecasting, 10, 606–619, https://doi.org/10.1175/1520-0434(1995)010%3C0606:AITDAA%3E2.0.CO;2, 1995.

Eyre, J. R., Brownscombe, J. L., and Allam, R. J.: Detection of fog at night using advanced very high resolution radiometer (AVHRR) imagery, Detect. fog night using Adv. Very High Resolut. Radiom. (AVHRR) imag., 113, 266–271, 1984.

Gultepe, I., Pagowski, M., and Reid, J.: A Satellite-Based Fog Detection Scheme Using Screen Air Temperature, Weather and Forecasting, 22, 444–456, https://doi.org/10.1175/WAF1011.1, 2007a.

Gultepe, I., Tardif, R., Michaelides, S. C., Cermak, J., Bott, A., Bendix, J., Müller, M. D., Pagowski, M., Hansen, B., Ellrod, G., Jacobs, W., Toth, G., and Cober, S. G.: Fog research: A review of past achievements and future perspectives, Pure Appl. Geophys., 164, 1121–1159, https://doi.org/10.1007/s00024-007-0211-x, 2007b.

Gultepe, I., Zhou, B., Milbrandt, J., Bott, A., Li, Y., Heymsfield, A. J., Ferrier, B., Ware, R., Pavolonis, M., Kuhn, T., Gurka, J., Liu, P., and Cermak, J.: A review on ice fog measurements and modeling, Atmospheric Research, 151, 2–19, https://doi.org/10.1016/j.atmosres.2014.04.014, 2015.

Gultepe, I., Sharman, R., Williams, P. D., Zhou, B., Ellrod, G., Minnis, P., Trier, S., Griffin, S., Yum, Seong. S., Gharabaghi, B., Feltz, W., Temimi, M., Pu, Z., Storer, L. N., Kneringer, P., Weston, M. J., Chuang, H., Thobois, L., Dimri, A. P., Dietz, S. J., França, G. B., Almeida, M. V., and Neto, F. L. A.: A Review of High Impact Weather for Aviation Meteorology, Pure Appl. Geophys., 176, 1869–1921, https://doi.org/10.1007/s00024-019-02168-6, 2019.

Jia, X., Lu, C., Liao, Z., Tian, P., Wang, Y., Wang, F., Yang, S., Dou, Y., Liu, X., and Liu, Y.: Comprehensive Analysis of the Relative Dispersion of Droplet-Size Distributions and Their Relationships to Key Physical Fog Processes Under Different Aerosol Conditions and Evolutionary Stages, Adv. Atmos. Sci., 43, 861–873, https://doi.org/10.1007/s00376-025-4228-9, 2026.

Ma, N., Zhao, C., Chen, J., Xu, W., Yan, P., and Zhou, X.: A novel method for distinguishing fog and haze based on PM2.5, visibility, and relative humidity, Sci. China Earth Sci., 57, 2156–2164, https://doi.org/10.1007/s11430-014-4885-5, 2014.

Mason, J.: The Physics of Radiation Fog, Journal of the Meteorological Society of Japan. Ser. II, 60, 486–499, https://doi.org/10.2151/jmsj1965.60.1_486, 1982.

Miller, M. R., Raftis, J. B., Langrish, J. P., McLean, S. G., Samutrtai, P., Connell, S. P., Wilson, S., Vesey, A. T., Fokkens, P. H. B., Boere, A. J. F., Krystek, P., Campbell, C. J., Hadoke, P. W. F., Donaldson, K., Cassee, F. R., Newby, D. E., Duffin, R., and Mills, N. L.: Inhaled

Nanoparticles Accumulate at Sites of Vascular Disease, ACS Nano, 11, 4542–4552, https://doi.org/10.1021/acsnano.6b08551, 2017.

Peng, J., Hu, M., Shang, D., Wu, Z., Du, Z., Tan, T., Wang, Y., Zhang, F., and Zhang, R.: Explosive Secondary Aerosol Formation during Severe Haze in the North China Plain, Environ. Sci. Technol., 55, 2189–2207, https://doi.org/10.1021/acs.est.0c07204, 2021.

Pope III, C. A. and Dockery, D. W.: Health Effects of Fine Particulate Air Pollution: Lines that Connect, Journal of the Air & Waste Management Association, 56, 709–742, https://doi.org/10.1080/10473289.2006.10464485, 2006.

Roach, W. T., Brown, R., Caughey, S. J., Garland, J. A., and Readings, C. J.: The physics of radiation fog: I – a field study, Quarterly Journal of the Royal Meteorological Society, 102, 313–333, https://doi.org/10.1002/qj.49710243204, 1976.

Sun, Y., Jiang, Q., Xu, Y., Ma, Y., Zhang, Y., Liu, X., Li, W., Wang, F., Li, J., Wang, P., and Li, Z.: Aerosol characterization over the North China Plain: Haze life cycle and biomass burning impacts in summer, Journal of Geophysical Research: Atmospheres, 121, 2508–2521, https://doi.org/10.1002/2015JD024261, 2016.

Twomey, S.: The Influence of Pollution on the Shortwave Albedo of Clouds, Journal of the Atmospheric Sciences, 34, 1149–1152, https://doi.org/10.1175/1520-0469(1977)034%3C1149:TIOPOT%3E2.0.CO;2, 1977.

Wagh, S., Krishnamurthy, R., Wainwright, C., Wang, S., Dorman, C. E., Fernando, H. J. S., and Gultepe, I.: Study of Stratus-Lowering Marine-Fog Events Observed During C-FOG, Boundary-Layer Meteorol, 181, 317–344, https://doi.org/10.1007/s10546-021-00670-w, 2021.

Wang, J., Wang, G., Wu, C., Li, J., Cao, C., Li, J., Xie, Y., Ge, S., Chen, J., Zeng, L., Zhu, T., Zhang, R., and Kawamura, K.: Enhanced aqueous-phase formation of secondary organic aerosols due to the regional biomass burning over North China Plain, Environmental Pollution, 256, 113401, https://doi.org/10.1016/j.envpol.2019.113401, 2020.

Wang, Q., Yamaguchi, R. T., Kalogiros, J. A., Daniels, Z., Alappattu, D. P., Jonsson, H., Alvarenga, O., Olson, A., Wauer, B. J., Ortiz-Suslow, D. G., and Fernando, H. J.: Microphysics and Optical Attenuation in Fog: Observations from Two Coastal Sites, Boundary-Layer Meteorol, 181, 267–292, https://doi.org/10.1007/s10546-021-00675-5, 2021.

Woo, S., Park, J., Lee, J.-Y., and Kweon, I. S.: CBAM: convolutional block attention module, Proceedings of the European Conference on Computer Vision (ECCV), 3–19, 2018.

Wu, J., Bei, N., Hu, B., Liu, S., Zhou, M., Wang, Q., Li, X., Liu, L., Feng, T., Liu, Z., Wang, Y., Cao, J., Tie, X., Wang, J., Molina, L. T., and Li, G.: Aerosol–radiation feedback deteriorates the wintertime haze in the North China Plain, Atmospheric Chemistry and Physics, 19, 8703–8719, https://doi.org/10.5194/acp-19-8703-2019, 2019.

Wu, Y., Liu, Q., Liu, D., Tian, P., Xu, W., Wang, J., Hu, K., Li, S., Jiang, X., Wang, F., Huang, M., Ding, D., Yu, C., and Hu, D.: Enhanced formation of nitrogenous organic aerosols and brown carbon after aging in the planetary boundary layer, npj Clim Atmos Sci, 7, 179, https://doi.org/10.1038/s41612-024-00726-x, 2024.

Yang, C., Clarke, K., Shekhar, S., and Tao, C. V.: Big Spatiotemporal Data Analytics: a research and innovation frontier, International Journal of Geographical Information Science, 34, 1075–1088, https://doi.org/10.1080/13658816.2019.1698743, 2020.

Zhong, J., Zhang, X., Dong, Y., Wang, Y., Liu, C., Wang, J., Zhang, Y., and Che, H.: Feedback effects of boundary-layer meteorological factors on cumulative explosive growth of PM2.5 during winter heavy pollution episodes in Beijing from 2013 to 2016, Atmospheric Chemistry and Physics, 18, 247–258, https://doi.org/10.5194/acp-18-247-2018, 2018.